


# Assessment of Substrate and TBC Damage Effects on Resonance Frequencies for Blade Health Monitoring

Jason van Dyke, University of Ottawa, Canada

 <https://orcid.org/0000-0002-7949-9072>

Michel Nganbe, University of Ottawa, Canada\*

## ABSTRACT

The reliability of critical aircraft components continues to shift towards onboard monitoring to optimize maintenance scheduling, economy efficiency, and safety. Therefore, the present study investigates changes in dynamic behavior of turbine blades for the detection of defects, with focus on substrate cracks and TBC spallation as they relate to vibration modes 1 to 6. Two-dimensional and three-dimensional finite element simulation is used. The results indicate that TBC spallation reduces natural frequencies due to the ensuing hot spot and overall increase in temperature, leading to drops in blade stiffness and strength. Cracks cause even larger frequency shifts due to local plastic deformation at the crack that changes the energy dissipation behavior. Mode 1 vibration shows the largest shifts in natural frequencies that best correlate to the size of defects and their position. As such, it may be most appropriate for the early assessment of the severity and location of defects.

## KEYWORDS

Blade Damage, Blade Health Monitoring, Damage Detection, Defect Location, Defect Size, Resonance Frequencies, Resonance Vibration, TBC Loss, Vibration Mode

## INTRODUCTION

The reliability of critical aircraft components continues to heavily rely on regular maintenance at pre-determined intervals. In addition, more difficult to inspect parts are often replaced independent of their damage state at the end of a pre-set service life. While achieving an unparalleled level of safety, this approach can lead to conservative maintenance schedules, unnecessary shutdowns, high maintenance costs and unforeseeable failures. Therefore, there is great need and growing drive to shift to more efficient maintenance through onboard monitoring in order to timely detect or replace damaged components while the defects are still at their incipient stage. In this context, the current study aims at conducting a comprehensive analysis of blade substrate and coating defects, together with the ensuing changes in blade temperature and properties, as they relate to shifts in blade natural frequencies. This is achieved by completing a series of FEA models, each with varying severity and location of damage, and comparing the results to those of the undamaged blade.

DOI: 10.4018/IJMMME.293222

\*Corresponding Author

This article published as an Open Access article distributed under the terms of the Creative Commons Attribution License (<http://creativecommons.org/licenses/by/4.0/>) which permits unrestricted use, distribution, and production in any medium, provided the author of the original work and original publication source are properly credited.

## BACKGROUND

The highly conservative approach currently used to ensure the safety of key aerospace components has led to parts, such as turbine blades, being among the most commonly rejected or replaced components (Carter, 2005). Therefore, current efforts primarily focus on detecting potential damages before they reach a critical size for rapid growth and component failure. However, most previous literature reports have focused on crack size and location, without accounting for the ensuing local hot spot and overall increase in blade substrate temperature. Moreover, little is reported on the effect of TBC coating loss or spallation on the resonance behavior of turbine blades. Operating in an extreme environment, turbine blades can be subject to a variety of damage mechanisms including: chattering, high cycle fatigue (HCF) from high frequency engine vibrations, low cycle fatigue (LCF) from extreme cold and hot phases, creep, corrosion, and foreign object damage (FOD), among others. To improve the performance and durability of turbine blades, advanced coating technologies have been developed and used for decades. Thermal barrier coatings (TBCs) are among the most performant protective systems (Padture et al., 2002; Sankar et al., 2019, Dhomne & Mahalle, 2016). Current turbine blade substrates are generally metal base, such as nickel base superalloys, and have lower temperature and corrosion resistance than TBCs. Therefore, substantial substrate temperature increases resulting from potential TBC loss can cause failure of the component within relatively few operational cycles. TBC damage mechanisms are complex and ultimate failure can result in the spallation of the top coat (Ali et al., 2018; Evans et al., 2001; Schlichting et al., 2003).

To further improve safety and economy efficiency while reducing downtimes, a great deal of efforts are currently being deployed to develop more robust, compact and efficient onboard monitoring systems (Yildirim & Kurt, 2018; Roemer & Kacprzynski, 2000; Mevissen & Meo, 2019). The goal is to continuously evaluate residual strength or health and to estimate the remaining service life of components (Boyd-Lee et al., 2001). Ongoing research efforts are making critical advances in monitoring approaches and sensing technology (Borovik & Sekisov, 2020; Sunar & Al-Bedoor, 2008; Ranjan, 2016). Non-contact sensors are favoured for the monitoring of turbine blade parameters to avoid interference with aerodynamic and structural performance (Procházka & Vank, 2011; Devi et al., 2021). Resonance vibrations are highly dependent on the design, microstructure, materials properties and damage state of blades (Efe-Ononeme et al., 2018; Pridorozhnyi et al., 2019; Prasad et al., 2017). As such, they are among the most reliable indicators of blade health. Particularly, shifts in resonance frequencies can be readily measured for the detection of potential blade damages (Djaidir et al., 2017; Madhavan et al., 2014; Atiyah & Falih, 2019; Rani et al., 2019). Therefore, the current study is based on a solid foundation of achievements realized so far. However, the work goes beyond blade cracks. It expands to not yet sufficiently studied aspects such as the effect of TBC damage on the dynamic behavior of turbine blades and how the impact of defects relates to specific mode shapes.

## MATERIALS AND METHODS

### System, Materials and Loading Conditions

The Pratt and Whitney PW-100 engine is used as reference in this study. Its inter-turbine temperature before the power stage is approximately 785°C and the exhaust temperature is between 565-600°C. Its further characteristics and main operation parameters are described in detail in the 2000 Pratt and Whitney Canada Large PW100 Series Training Manual and in earlier publications (van Dyke & Nganbe, 2021; Hosking et al., 1999; Saravanamuttoo, 1987). Cruise loading condition at 85% of the maximum propeller shaft rotation speed of 1200 rpm is taken as basis for the simulation. Waspaloy IN713LC is considered as blade substrate (Donachie & Donachie, 2002) with temperature dependent elastic modulus and strength.

In a first step of modelling, elastic-plastic material behavior is considered and the blade is modelled as a two-dimensional solid of 100 mm height and 10 mm thickness. A first partition is added for a

cooling channel at the blade center as illustrated in Figure 1(a). Two further partitions are added for the thermal barrier coating (TBC) layer at the surface on both the pressure and suction sides as shown in the magnified image in Figure 1(b). The TBC thickness is taken as 300  $\mu\text{m}$ , which is among the thickest recorded in literature (Padture et al., 2002). The thermal barrier coating is simplified into a single defect free  $\text{Y}_2\text{O}_3$ -stabilized  $\text{ZrO}_2$  (YSZ) top coat layer with an elastic modulus between 10 and 50 GPa (Padture et al., 2002; Xu et al., 2004).

In a second step, 3D modelling is conducted also using elastic-plastic material behavior to investigate potential effects of three-dimensional variations in blade geometry. Due to the much higher complexity of three-dimensional modelling however, it is limited to notches that proved to have the strongest effect on natural frequencies as per the two-dimensional models. The investigation is focused on the effect of varying notch depth at midspan, as well as on the position of a notch of constant depth in term of distance from the blade root along the blade span. The models are created by modifying an initial stock Sokolov profile in Airfoil Design Workshop. It is then scaled up to the final blade geometry in Solidworks with simple fir tree design, 80 mm height (not including the root), 21 mm width (leading edge to trailing edge), and 3.2 mm thickness at its thickest point as shown in Figure 2.

Three average median blade temperatures are studied: 755, 955 and 1155 K. The temperature of the blade is allowed to reach steady state in initial FEA heat transfer models. The resulting nodal

**Figure 1. Two-dimensional model geometry: (a) blade with internal cooling channel at the center; (b) magnified half of the blade model showing the TBC coating at the surface with finer mesh (left), and the center with larger mesh (right)**

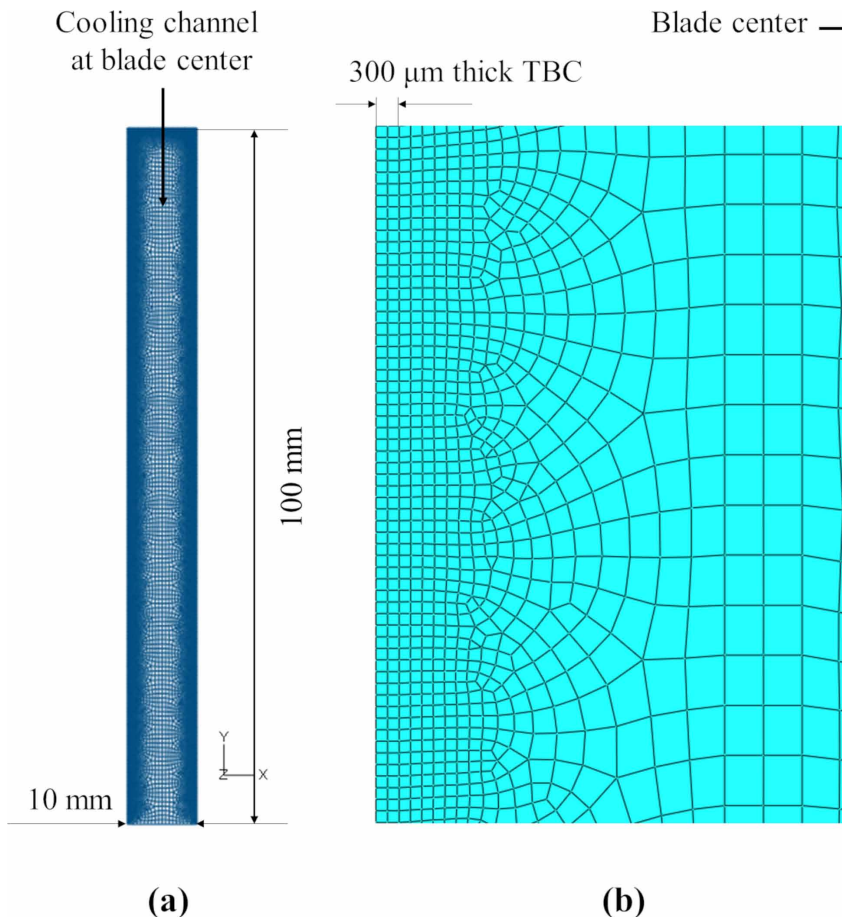
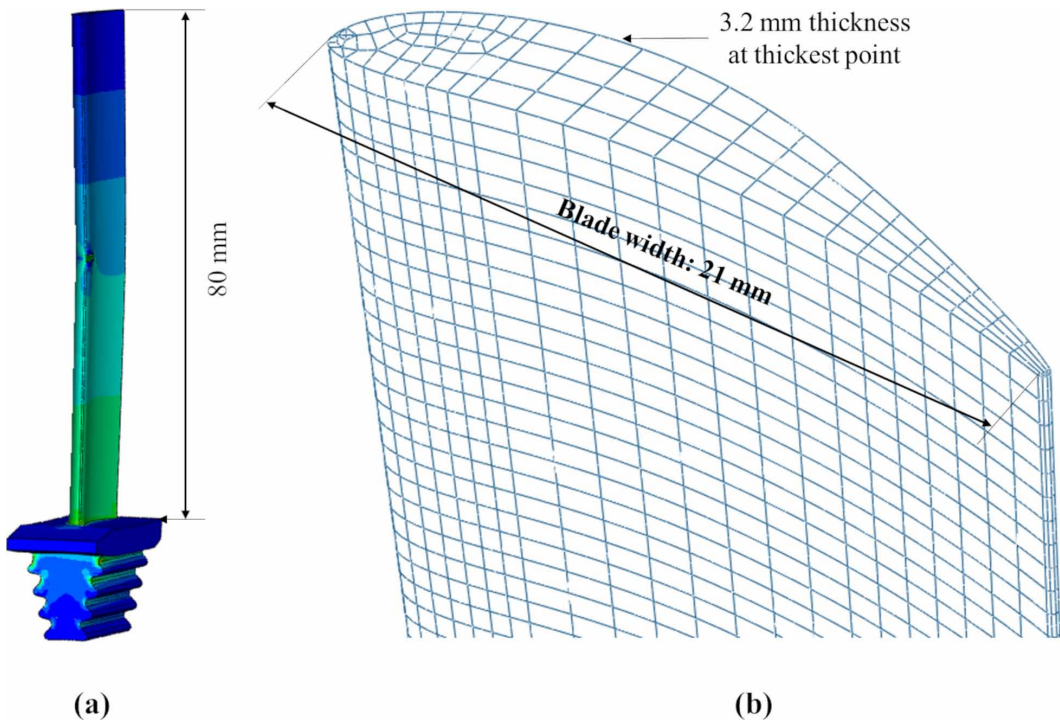


Figure 2. Three-dimensional model geometry: (a) blade with fir tree design; (b) magnified view showing the thickness variation along the width of the blade, and the used mesh



temperature distributions are then exported to the structural model for linear perturbation frequency extraction and subsequent analysis. Two different types of defects are introduced, namely TBC loss representative for coating spallation, and notches, representative for surface cracks. The size of TBC defects and the depth of notches are varied to study the effects of damage severity as illustrated later in the Results section. Moreover, the defects are placed at different distances from the blade root along the blade span to study the effect of damage location.

### Two-Dimensional FEM Modelling, Meshing and Convergence Study

The natural frequencies are calculated within Abaqus using its inbuilt Lanczos eigensolver. The analysis is limited to the first 6 modes of vibrations. Meshes are kept similar in both heat transfer and structural models to insure accurate transfer of nodal temperature data. In general, the heat transfer solution is less sensitive to mesh size. Thus, the mesh size optimization and the convergence study are done for the structural models only. Meshing optimization is initiated starting from the two main characteristic blade partitions, the surface and the center. Specifically, a structured meshing algorithm is used at both the blade surface and center with element sizes of  $300\text{ }\mu\text{m} \times 300\text{ }\mu\text{m}$  and  $1\text{ mm} \times 1\text{ mm}$ , which correspond to the thicknesses of the TBC coating and the cooling channel, respectively. A free meshing algorithm is then applied everywhere else to achieve a smooth transition from the smaller elements in the TBC to the larger elements at the cooling channel as illustrated earlier in Figure 1. Convergence study is then conducted using mode 1 vibration and linear elements by progressively reducing the element sizes across the blade to investigate potential improvements in modelling results. As seen in Table 1, the estimated natural frequency value stabilized around 686 Hz for the undamaged blade. This is achieved with an element edge size of  $1.5 \times 10^{-4}\text{ m}$  at the surface to obtain

Table 1. Convergence study for two-dimensional modelling

Node Count		Mode 1 Natural Frequency [Hz]	Node Count		Mode 1 Natural Frequency [Hz]	
Undamaged blade	5771	685.194	Blade with 3 mm deep crack at midspan			
	19401 (used for study)	685.885		21909 (used for study)	669.604	
	57620	686.118		65016	669.796	
	94857	686.116		92349	669.745	
	283858	686.116		275627	669.789	
	289341	685.885				

two elements within the TBC coating, and an element edge size of  $5.1 \times 10^{-4}$  m at the center to also obtain two elements at the close proximity to the cooling channel, defined as a 1 mm wide partition at the center of the blade. This resulted in 19401 nodes forming 18819 mesh elements as used in this study. 18558 of the elements are linear quadrilateral of type CPE4R for structural analysis and of type DC2D4 for heat transfer analysis, while the remaining 261 elements are of linear triangular type. CPE elements are bilinear plane strain elements with reduced integration hourglass control. DC2 elements are simple linear heat transfer elements. The undamaged model is created and analysed to provide a baseline mechanical response. Subsequently, damages are introduced to study changes in response. TBC defects, representative for coating spallation, are created on the pressure side of the blade over the entire coating thickness by locally applying the cut-extrude feature to the TBC partition. Similarly, notches with 1.5 mm tip radius are introduced on the pressure side of the blade. This required a further refining of meshes around the cracks as described in an earlier publication (van Dyke & Nganbe, 2021). As seen in Table 1 for a 3 mm deep crack for example, the estimated natural frequency values are stable beyond 21909 nodes, which is used in this work. The specific number of meshes varied slightly depending on the specific size of the crack.

### Three-Dimensional FEM Modelling, Meshing and Convergence Study

3D modelling is more complex and time consuming. Therefore, it is limited to primarily serve the verification of tendencies observed in the two-dimensional models. As such, relatively coarse meshes are used to achieve a balance between modelling accuracy and processing time. For meshing optimization, a comparison is conducted on an undamaged blade between linear elements with 31836 nodes and quadratic elements with 120497 nodes. A substantial difference in processing time was observed, 2-3 hours for the linear model compared to 5-6 hours for the quadratic model. However, the latter yielded considerable improvement in modelling accuracy, rationalising the use of quadratic elements despite their longer processing time. They are 25082 hexahedral elements of type C3D20R for structural analysis, and of type DC3D20 for heat transfer analysis. The remaining 1826 are linear tetra elements, namely C3D15 for structural and DC3D15 for heat transfer modelling. C3D denotes a general stress/displacement element with hourglass control. DC3 denotes general 3D heat transfer/mass diffusion elements. Three-dimensional damages in the form of notches with circular tip are then also introduced. They are created with varying depths and positioned at different distances from the blade root using the cut revolve feature in Abaqus as described earlier (van Dyke & Nganbe, 2021). Finer meshes are used around notches similar to the two-dimensional models, leading to increased element counts depending on the type and size of the defects. For a 1.1 mm deep notch for instance, the used number of quadratic meshes increased to a node count of 156966.

## RESULTS

### Two-Dimensional Modelling of TBC and Substrate Damage

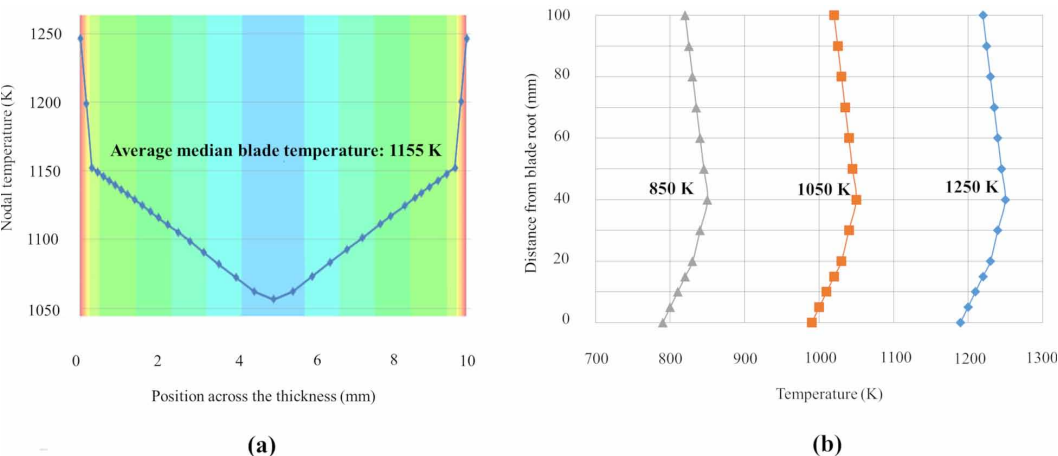
Illustratively, the temperature distribution across the thickness of the undamaged blade at midspan is shown in Figure 3(a) for the highest investigated average median temperature of 1155 K. The strong temperature drop across the protective TBC coating, followed by a softer drop towards the cooling channel at the blade center can be seen, which is expected from fundamentals of heat transfer.

Figure 3(b) shows the corresponding surface temperature profiles along the blade span for the 3 considered temperature levels with the highest values of 850 K, 1050 K and 1250 K measured around midspan. Due to the loss of coating protection, TBC spallation and notches or cracks cause a temperature hot spot at the blade surface as illustrated in Figure 4(a) and (b), respectively. The hot spot also leads to an overall increase in average blade temperature by about 52 K.

The base state without any TBC defect or notch and the first 6 two-dimensional vibration mode shapes are illustrated in Figure 5. The calculated corresponding natural frequencies for the different investigated surface temperature conditions are summarized in Table 2. The natural frequencies can be seen to increase with increasing mode of vibration. Furthermore, the natural frequencies drop with increasing temperature. The drop is strongest at 1155 K due to a transition in mechanical behavior of the blade from primarily dislocation slip at lower temperature to mainly easier creep deformation processes at higher temperatures. This transition leads to a strong decrease in material resistance to deformation, particularly in yield strength (van Dyke & Nganbe, 2021; Nganbe & Fahim, 2010; Nganbe, 2014; Nganbe, 2009). Consequently, the energy dissipation properties and damping behavior of the blade change, leading to lower natural frequencies.

The analysis of frequencies allows assessing how close they are to the excitation frequency during use and, thus, the probability of a blade falling into resonance vibration. The excitation of a turbine blade is largely due to its rotation and the cyclic variation of gas moving across the blade surface, at frequencies equal to the rate at which the blades pass behind the guide vanes. The turbine stage of the considered PW-100 engine has 74 blades as indicated in the 2000 Pratt and Whitney Canada Large PW100 Series Training Manual and reported earlier (Hosking et al., 1999). In this study, it is taken to rotate at the cruise speed of 1500 rad/s (238 rev/s). The excitation frequency can then be calculated as  $238 \times 74 = 16950$  Hz. Comparing with Table 2, it can be seen that the excitation frequency lies between those of the fourth and fifth modes and none of the found natural frequencies

**Figure 3. Temperature profiles: (a) across the blade thickness at midspan for the highest investigated average median temperature of 1155 K, corresponding to the highest surface temperature of 1250 K; (b) at the blade surface along the span with highest values measured around midspan for the three investigated temperature levels**





**Figure 4. Local hot spot and temperature distribution as a result of defects as estimated using two-dimensional modelling: (a) TBC defects at varying locations along the blade span; (b) notch representative for blunted crack**

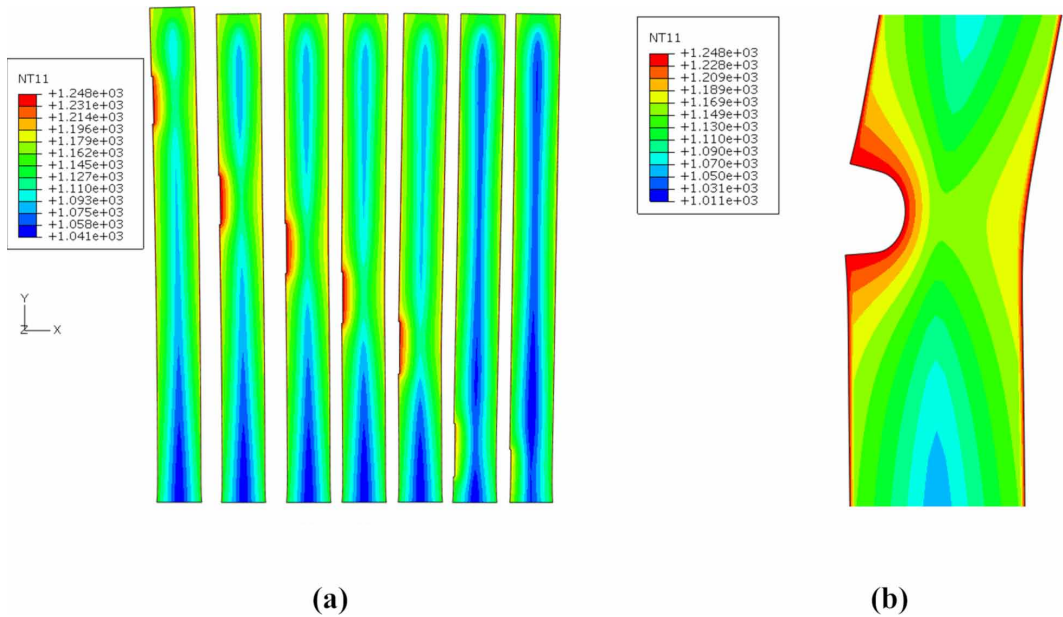
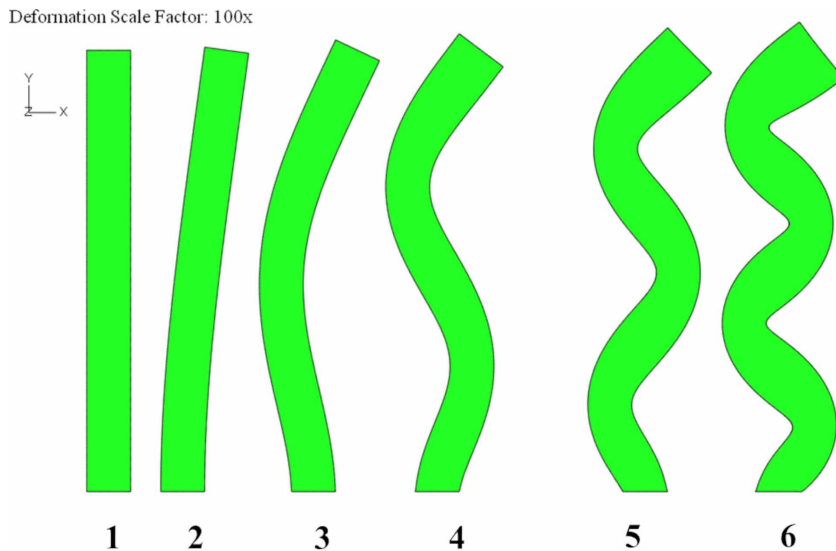


**Figure 5. Base state of the first 6 two-dimensional vibration mode shapes without any TBC defect or notch**



is critically close to resonance or chatter under cruise operation conditions for the undamaged blade. This result can be expected from a successful engineering design, as avoiding resonance vibration is a key criterion for safe operation. However, as natural frequencies are seen to drop with increasing temperature, the localized exposure of the blade substrate resulting from TBC defects and notches or cracks can be expected to lead to vibration frequency shifts.

**Table 2. Natural frequencies for the first 6 modes of vibrations of the undamaged blade as obtained from two-dimensional modelling**

Mode	Natural Frequency (Hz)		
	755 K	955 K	1155 K
1	748	721	686
2	4497	4329	4119
3	11899	11456	10897
4	12242	11785	11186
5	21730	20921	19896
6	33287	32048	30472

### *Shifts in Blade Natural Frequencies Due to TBC Defects*

TBC spallation changes the steady state temperature distribution with a hot spot at the defect. The temperature also rises in the interior of the blade, which is found to have a small, but measurable effect on natural vibration frequencies. In the case of TBC damage located at midspan for instance, the natural frequencies decrease for practically all modes of vibrations with growing TBC defect size as shown in Figure 6. This is primarily due to a decrease in elastic modulus resulting from increased blade temperature. As a worse case scenario, the change in natural frequencies from a perfectly undamaged blade to one with completely no TBC coating on the pressure side is considered. It is found that the greatest shift in natural frequencies takes place in the first mode of vibration. This occurs at the highest investigated average median temperature of 1155 K and creates a vibration frequency drop by 1.76%. The smallest relative frequency drop is observed in the fourth mode of vibration at the lowest investigated average median temperature of 755 K, and is 0.32%.

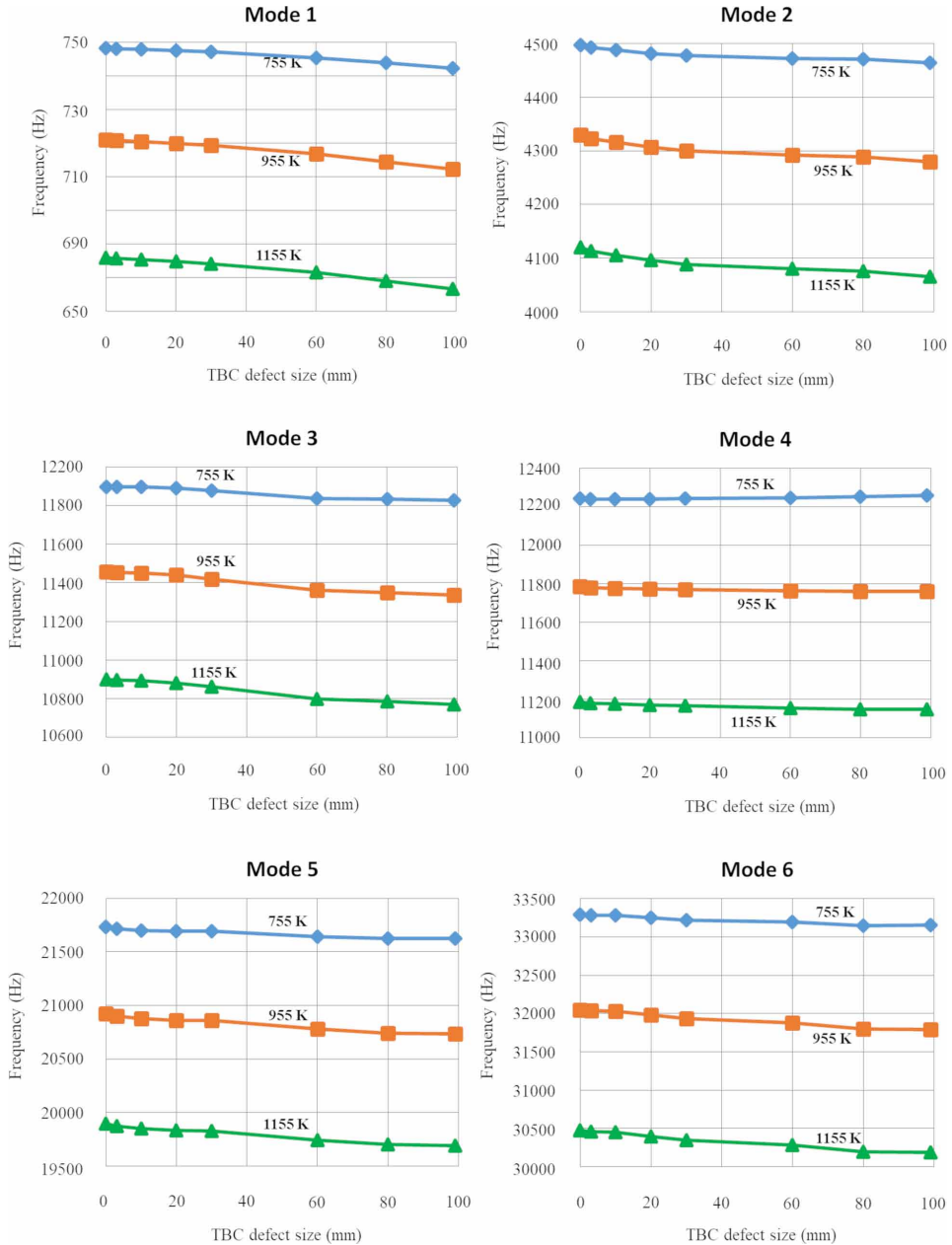
Moreover, the location of the TBC defect has a measurable effect on the natural frequencies as illustrated in Figure 7. As the defect is moved from the root to the tip of the blade, changes in natural frequencies are observed that strongly depend of the specific mode of vibration. The largest change occurs within the first mode of vibration at the highest investigated average median blade temperature of 1155 K. In this case, the natural frequency is found to increase by 1.23% when a 10 mm TBC defect is moved from the root (with center at 5 mm from the root) to near the tip (with center at 80 mm from the root) of the blade, which represents a shift by 7.5 Hz. The natural frequencies tend to also increase slightly for mode 4, while modes 2, 3, 5 and 6 tend to fluctuate with only moderate overall changes.

### *Shifts in Blade Natural Frequencies Due to Notches or Cracks*

An increase in blade temperature also occurs around a notch or crack where the substrate is exposed directly to the applied surface temperature due to missing TBC protection. In addition, cracks locally reduce the blade stiffness and strength due to local geometry changes and stress concentrations. As a result, the natural frequencies decrease steadily as cracks grow in size by propagating into the blade. The rate of change and the overall variation depend on each specific vibration mode. The percent changes with reference to an undamaged blade for the first 6 vibration modes are illustrated in Figure 8. In increasing order, mode 1, mode 5 and mode 2 are the most sensitivity to crack propagation with natural frequency drops by around 5.8%, 9.1% and 16.8%, respectively, with the blade temperature having only little effect on the relative changes. Moreover, Figure 9 shows the impact of a 3 mm deep notch location on natural frequencies. As the notch is moved along the blade span from the root to the tip, the natural frequencies can be seen to fluctuate with peaks and valleys that tend to coincide with the nodes and anti-nodes of the respective vibration modes.

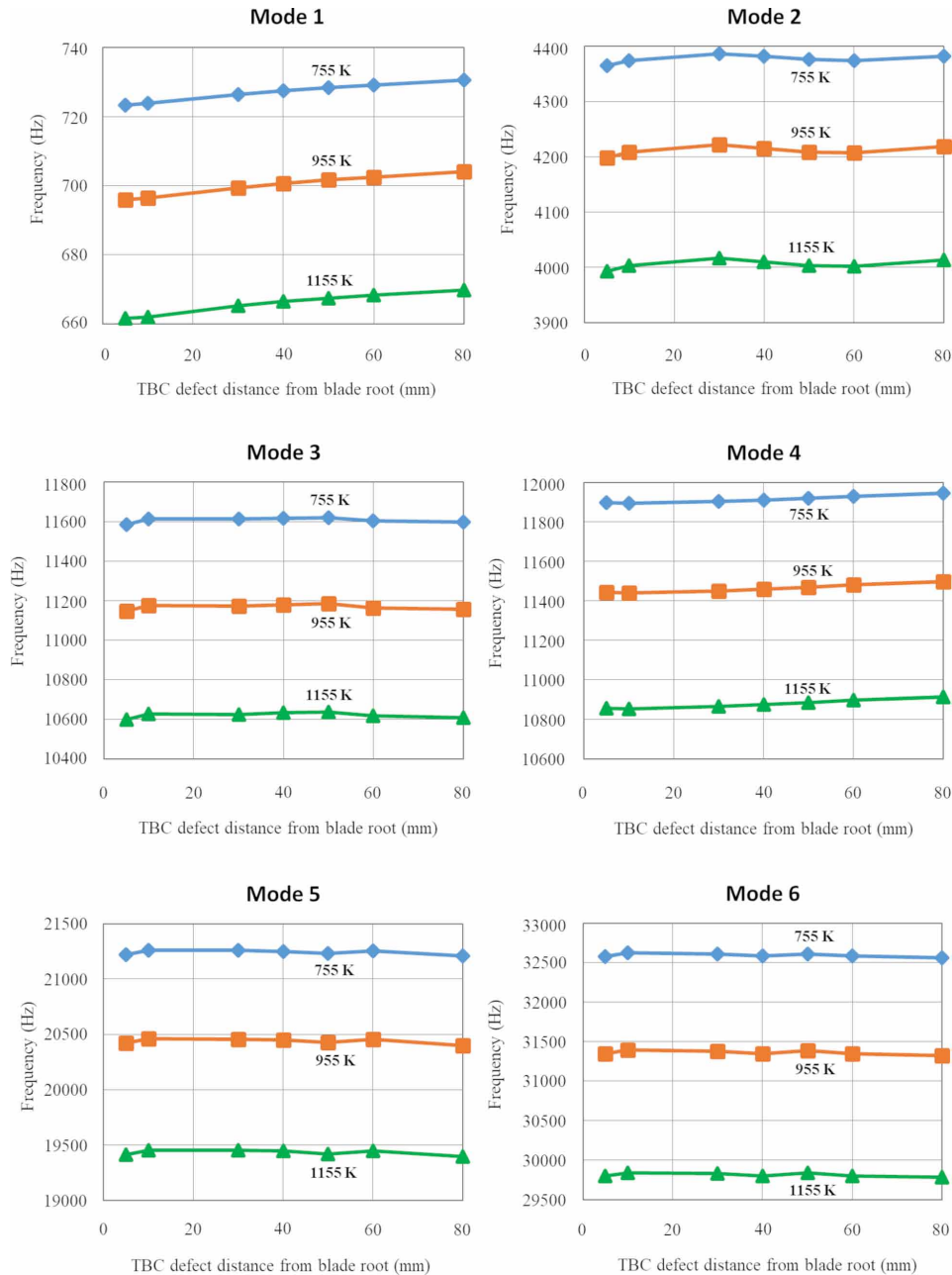


**Figure 6. Variation of natural frequencies with midspan TBC defect size for the first 6 modes of vibrations as estimated using two-dimensional modelling**



Overall, mode 1 vibration with the simplest shape shows the largest percentage frequency changes with a low of about 581 Hz at 5 mm from the blade root. The natural frequencies then reverse to continuously increase towards the blade tip. For the highest investigated average median temperature of 1155 K, the variation from the minimum value at the low to the value when the notch is located at 80 mm from the blade root is about 22%. The other vibration modes undergo lower relative changes between their minimum and maximum frequency values as they fluctuate. In increasing order, the

**Figure 7. Variation of natural frequencies for the first 6 modes of vibrations with 10 mm size TBC defect location expressed in term of distance from the blade root as estimated using two-dimensional modelling**

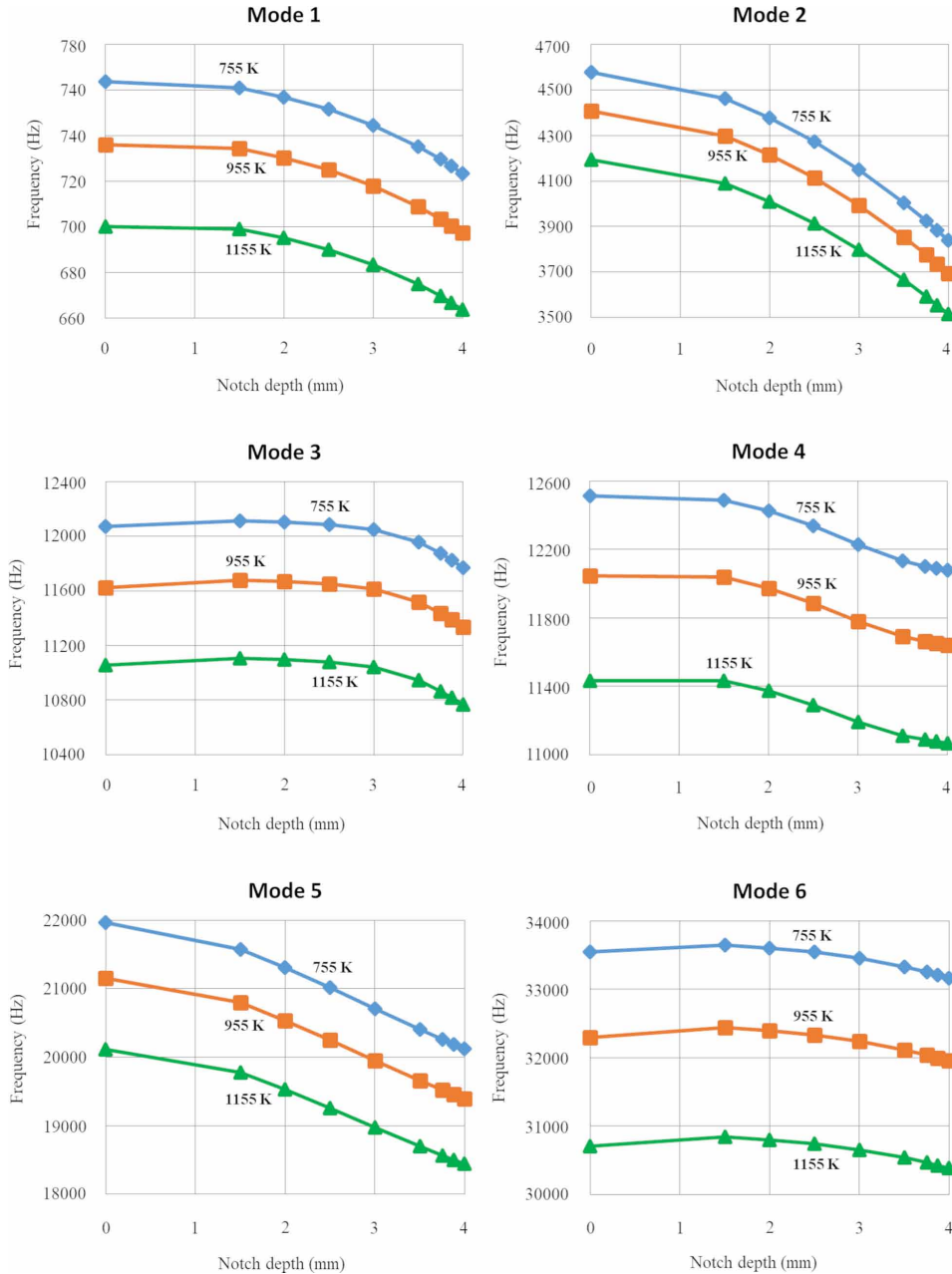


relative changes are around 3.9%, 5.9%, 9.1%, 9.9% and 10.8% for mode 4, mode 6, mode 5, mode 3 and mode 2, respectively.

**Three-Dimensional Modelling of Notches**

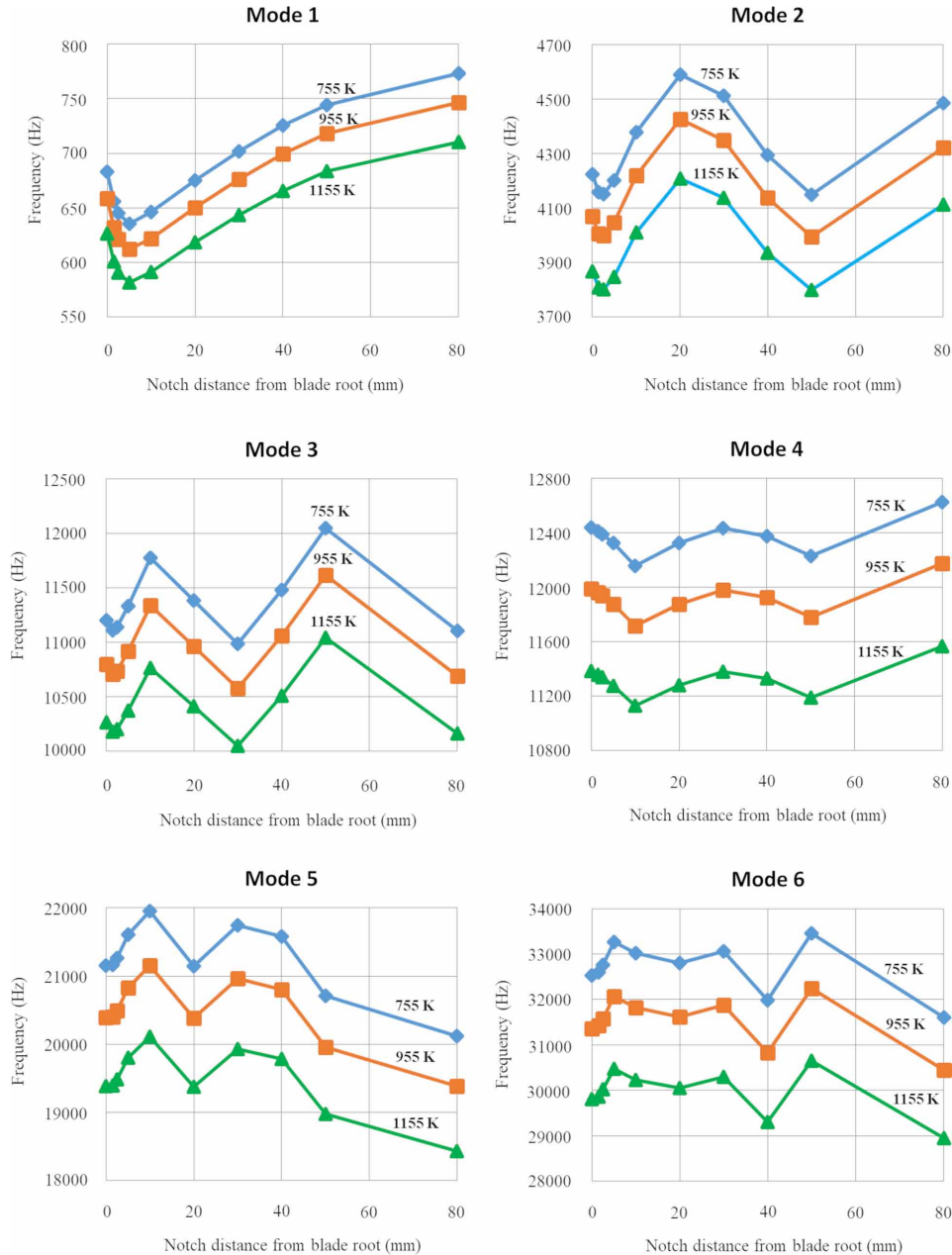
Overall, lower natural frequencies are obtained with three-dimensional modelling as compared to the two-dimensional models primarily due to discrepancies in model geometries. Specifically, the notch

**Figure 8. Variation of natural frequencies with midspan notch depth for the first 6 modes of vibrations as estimated using two-dimensional modelling**



depth varies along the blade width, as does the blade thickness, in the three-dimensional models. For the sake of simplicity however, the three-dimensional models use the largest notch depth that occurs at the thickest blade location close to the leading edge where potential cracks are most likely to initiate. This approach overestimates the overall notch size, making the effective severity of damage substantially lower as compared to the two-dimensional models that assume a constant notch depth across the entire width of the blade. However, notwithstanding the differences in blade geometry, notch

Figure 9. Variation of natural frequencies for the first 6 modes of vibrations as a function of the location of a 3 mm deep notch with 1.3 mm tip radius expressed in term of distance from the blade root as estimated using two-dimensional modelling



size, and ensuing absolute magnitudes of frequencies and their shifts, three-dimensional modelling confirms the trends observed earlier from the two-dimensional models. Namely, the natural frequencies decrease with increasing notch depth as illustratively summarized in Table 3 for the average median blade temperature of 1155 K. Similar shifts are observed at the two other investigated temperature levels of 955 K and 755 K, although to a lesser magnitude. The largest decrease exits in mode 3

**Table 3. Natural frequencies as a function of midspan notch depth as obtained from three-dimensional modelling considering elastic-plastic material behavior and 1155 K average median blade temperature**

Notch depth (mm)	Natural Frequency (Hz)					
	Mode 1	Mode 2	Mode 3	Mode 4	Mode 5	Mode 6
0	345	1730	2104	2509	5655	7175
0.6	345	1730	2093	2510	5664	7188
0.9	344	1727	2070	2504	5651	7168
1.1	344	1728	2053	2501	5653	7166

vibrations. This is the equivalent mode shape to mode 2 in the two-dimensional model. Moreover, the natural frequency shifts depend on the defect location along the blade span.

## DISCUSSION

### Validation of Simulation Results

For validation, the current study is compared to existing literature on Nickel base superalloy gas turbine blades as summarized in Table 4. For this purpose, the three-dimensional models are considered, as they have the closest similarity to experimental and application set-ups. Also, the undamaged blade state is used for which sufficient comparable literature data are available. It can be seen that the results agree considerably well. Specifically, all studies show increasing natural frequency values with increasing vibration mode number. However, discrepancies ranging from 26% to 160% can be observed within identical modes between the different studies. Such discrepancies can be expected given variations in loading parameters, including differences in turbine engine models, operating conditions, blade material, blade dimensions, blade fixation and exposure temperature.

**Table 4. Natural frequency values for Nickel based superalloy turbine blades as determined in this study and in previous literature**

Work	Blade Material	Temperature (K)	Natural Frequency (Hz)					
			Mode 1	Mode 2	Mode 3	Mode 4	Mode 5	Mode 6
Current study (Theoretical)	IN713LC	1155	345	1730	2104	2509	5655	7175
Madhavan et al., 2014 (Theoretical)	CM – 247 LC	Room temperature	401					
Efe-Ononeme et al., 2018 (Theoretical)	U500	Not provided	897	1857	3173	4378	5515	7376
	IN738	Not provided	752	1533	2618	3622	4555	6092
Rani et al., 2019 (Theoretical)	IN738LC	Room temperature	485	1465	1943	2151	3221	3710
Rani et al., 2019 (Experimental)	IN738LC	Room temperature	484	1475	1935	2130	3190	3690

## **Dependence of Natural Frequencies on Temperature, Defect Size, Defect Location, and Vibration Mode**

The vibration frequencies decrease with increasing temperature. This is in agreement with fundamental theory and is the result of a decrease in elastic modulus and corresponding decrease in stiffness. Both investigated defect types also lead to changes in natural frequencies. As TBC defects grow in size, all natural frequencies decrease, with some modes proving more sensitive to defects at certain locations than others. Also, simulation results indicate increased sensitivity of natural frequencies to TBC spallation at higher temperatures where the elastic modulus is lower. As a result, changes caused by defects represent a larger percentage drop in elastic modulus, and consequently in natural frequencies. Overall however, the shifts in natural frequencies caused by TBC loss are relatively small, often below 2%, which may require more performant sensors with increased resolution for their reliable detection, particularly when considering potential vibration noises.

Although the overall frequency changes of the second mode of vibration with shifts in the range of 1.1% are less than those of the first mode with shifts around 1.76%, the second mode shows higher defect sensitivity at smaller TBC spallation sizes. This indicates that measuring the vibration characteristics of the second vibration mode may be of greater use for early detection of TBC damage. For mode 1 vibrations, the natural frequencies consistently decrease as the TBC defect and the ensuing local hot spot approach the root of the blade. The fourth mode behaves in a similar fashion, although with lower sensitivity. As such, tracking natural frequency shifts of mode 1, and to a certain extent mode 4, could help assessing locations of potential TBC loss during blade health monitoring and maintenance. Modes 2, 3, 5 and 6 vibrations are also sensitive to TBC defect location, but do not change in a consistent manner. As such, tracking their changes may not be ideal for assessing the TBC defect position as their observed shifts do not continuously correlate with the distance along the blade span, with only occasional peaks and valleys. For example, minimum natural frequency values are observed in the second mode of vibration at two TBC defect locations: 5 mm and 60 mm from the blade root. For mode 5, minimum natural frequencies occur at 5 mm, 50 mm, and 80 mm from the blade root.

Similar to the effects of TBC defects, growing notches or cracks cause an increasing drop in all natural frequencies, particularly for mode 1 and mode 2 vibrations with the largest percentage drops. In addition, these two first modes are more likely to have the largest measurable vibration amplitudes due to their relatively simple mode shapes. Therefore, they show the greatest potential for detecting and quantifying the severity of blade substrate damage. As the notch is moved along the blade span, the natural frequencies of mode 1 undergo a minimum at 5 mm from the root and then reverse to increase continuously as the notch location moves further towards the tip. As such, mode 1 vibrations may also be the most appropriate for assessing the location of blade defects for monitoring and maintenance. For the investigated 3 mm deep notch with 1.5 mm tip radius, 5 mm was determined as the minimum distance from the blade root that allows the entire plastic deformation zone at the notch tip to be completely contained within the blade. At the same time, the overall mechanical loading of the blade, caused by both the centrifugal force and the gas pressure bending moment, increases from the tip to the root of the blade. This combination of increasing mechanical loading towards the blade root and the given maximum size of the crack tip plastic deformation zone produces the strongest drop in blade stiffness and strength for notches located at 5 mm from the blade root. For notches closer to the blade root, the plastic zone narrows primarily due to higher local material strength resulting from lower local temperature in the immediate proximity to the colder fixation area at the rotor. The resulting drop in cyclic local plastic deformation leads to changes in energy dissipation, causing the natural frequencies to rise towards the blade root for notch locations within 5 mm to its proximity. For the other investigated modes of vibrations 2 to 6, the dependence of natural frequencies on notch location is more complex with lows and highs observed as the defect position moves from the root to the tip of the blade. The lows and highs can be correlated to critical positions in the mode shapes, specifically to nodes and anti-nodes. As such, the analysis of higher modes of vibrations may not be



efficient for predicting the notch or crack location. Instead, modes 2 to 6 could potentially be more useful as supplements to mode 1, particularly for a more refined prediction of defect location.

### **Potential for Monitoring TBC and Blade Damage Using Resonance Vibration Measurements**

The excitation of a turbine blade is largely due to the cyclic variation of gas moving across the blade's surface. None of the extracted natural frequencies approaches the estimated excitation frequency of 16950 Hz, the closest to resonance being in modes 4 and 5 with natural frequencies of 11186 and 19896 for the undamaged blade at the highest investigated average median temperature of 1155 K, respectively. At this same temperature however, the natural frequency of mode 5 decreases by approximately 1810 Hz as the notch size progresses to a depth of 4 mm at midspan. This is the largest notch size considered in this study, with deeper midspan notches resulting in infinite deflection indicating potential blade fracture (van Dyke & Nganbe, 2021). The drop brings the mode 5 natural frequency to 18086 Hz, representing about 9.1%, still 1136 Hz higher than the estimated excitation frequency. However, the frequencies of mode 5 vibrations are observed to further fluctuate with lows representing a further drop by another 8.3% as the notch location is moved along the blade span. This brings the natural frequency of the lows down to 16439 Hz, well within the range of the excitation frequency of 16950 Hz. Therefore, it can be concluded that, the growth of relatively small cracks into the blade would generally not change the natural frequencies sufficiently to cause any resonance vibration at cruise operation considered at 85% of the maximum turbine rotation speed. However, large cracks with depths in the range of 4 mm could well cause resonance of the blade when located at critical positions such as nodes and anti-nodes, particularly for mode 5 vibrations. Moreover, excitations at transient states of turbine operation can pass through or be closer to blade natural frequencies, particularly during higher loading stages such as takeoff and landing. In fact, the maximum propeller rotation speed of the reference Pratt and Whitney PW-100 turbo prop is given as 1200 rpm. Using a gear ratio of 17/1, a maximum power stage rotation speed of 340 rev/s can be calculated, which would correspond to a potential excitation frequency of 25160 Hz considering the 74 blades in the stage. This suggests that the excitation frequency could well vary beyond the modelled cruise natural frequency range of mode 5, and approach the mode 6 natural frequency of 30472 Hz, as determined in the two-dimensional model. Therefore, resonance vibrations of blades can be expected even under normal turbine operating conditions, which is often addressed using appropriate dampers (Giridhar et al., 2012; Gastaldi et al., 2018). Furthermore, resonance vibrations of turbine blades in particular, and vibration characteristics of critical components in general, have proven to be a good overall metric for assessing the health of components (Hou et al., 2002; Al-Bedoor et al., 2006; Farrar et al., 2021). Consequently, monitoring natural frequencies is one of the key approaches to estimate the severity of loading and to assess the fatigue and remaining service life of blades. Specifically, monitoring natural frequency shifts has become a viable way for the detection of potential cracks for blade health monitoring. The current study confirms this trend by suggesting natural frequency variations by up to 22% as blade substrate defects grow in size or vary in position. This range of change is readily detectable using current sensors. Moreover, the study suggests that as novel sensors continue to increase in capacity, robustness, resolution and performance, timely detecting and monitoring TBC coating defects could also become possible despite the much smaller shifts they cause in natural frequencies.

The correlations between blade defects and natural frequencies can be rationalized by the capacity of damage in the form of TBC loss and substrate cracks to cause local hot spots and overall increase in blade substrate temperature. This causes the local and overall effective blade stiffness to decrease, which, together with stress concentrations in the case of cracks, produces changes in energy dissipation properties. The result is a change in the dynamic response of the system, generally leading to lower natural vibration frequencies and to larger vibration amplitudes (Farrar et al., 2021). The described

relationships can be illustrated as in Equation (1) by simplifying the blade and considering it as a cantilevered beam of stiffness  $k$  (Palm, 2007):

$$k = \frac{Ewh^3}{4L^3} \quad (1)$$

where  $E$  is the elastic modulus;  $w$  is the width;  $h$  is the thickness; and  $L$  is the length of the beam. The undamped natural frequency  $\omega_n$  of a linear system can then be estimated as in Equation (2) (Palm, 2007):

$$\omega_n = \sqrt{\frac{k}{m}} \quad (2)$$

where  $m$  is the mass of the system.

## CONCLUSION

The current study investigates the impact of defects in both substrate and TBC coating on the blade natural frequencies, with the following main conclusions:

1. TBC spallation results in drops in natural frequencies. This is primarily because of the ensuing hot spot on the blade substrate and overall increase in blade temperature, leading to reduced elastic modulus and strength. However, the drops in natural frequencies due to TBC defects are below 2%, making them potentially more difficult to detect and monitor than cracks.
2. In addition to reduced stiffness and strength due to increased blade substrate temperature, considerable local plastic deformation can occur at notches, representative for blunted cracks, due to stress concentrations. This can change the energy dissipation of the blade considerably, making the detection of cracks more reliable.
3. The shifts in natural frequencies depend on defect location with lows and highs at nodes and anti-nodes of the different vibration mode shapes.
4. The two-dimensional models suggest that cracks can cause variations in blade natural frequencies by up to 22%, which is well measurable using current sensors. The three-dimensional models confirm the trend of the two-dimensional models, but the natural frequency levels are lower and the shifts are smaller at all modes of vibrations. The discrepancies are primarily due to the assumption of constant thickness and notch depth in the two-dimensional models, while the three-dimensional models replicated the shape of the blade more realistically with the thickness and notch depth varying along the width.
5. In summary, the blades have to pass through resonance frequencies, particularly during acceleration and deceleration phases, such as engine starts and shutdowns. This allows using appropriate sensors to measure shifts in natural frequencies to assess the position and severity of blade coating and substrate defects for the health monitoring of turbine blades.

## ACKNOWLEDGMENT

This research was supported by the National Science and Engineering Research Council of Canada [NSERC Discovery Grant number: 210487-180599-2001].

## REFERENCES

- Al-Bedoor, B. O., Aedwesi, S., & Al-Nassar, Y. (2006). Blades condition monitoring using shaft torsional vibration signals. *Journal of Quality in Maintenance Engineering*, 12(3), 275–293. doi:10.1108/13552510610685110
- Ali, R., Shehbaz, T., & Bemporad, E. (2018). Investigation on failure in thermal barrier coatings on gas turbine first-stage rotor blade. *Journal of Failure Analysis and Prevention*, 18(5), 1062–1072. doi:10.1007/s11668-018-0530-5
- Atiyah, Q. A., & Falih, M. R. (2019). Experimental and numerical study of the crack position and depth effects on natural frequencies of turbine blades. *Journal of University of Babylon for Engineering Sciences*, 27(3), 332–344.
- Borovik, S., & Sekisov, Y. (2020). Single-coil eddy current sensors and their application for monitoring the dangerous states of gas-turbine engines. *Sensors (Basel)*, 20(7), 2107. doi:10.3390/s20072107 PMID:32276496
- Boyd-Lee, A. D., Harrison, G. F., & Henderson, M. B. (2001). Evaluation of standard life assessment procedures and life extension methodologies for fracture-critical components. *International Journal of Fatigue*, 23(1), 11–19. doi:10.1016/S0142-1123(01)00116-5
- Carter, T. J. (2005). Common failures in Gas turbine blades. *Engineering Failure Analysis*, 12(2), 237–247. doi:10.1016/j.engfailanal.2004.07.004
- Devi, P. T., Kumar, S., Pratap, D., Shylaja, S., Satish, T. N., & Vishwanatha Rao, A. N. (2021). Rotor blade vibration measurement on aero gas turbine engines. In C. Mistry, S. Kumar, B. Raghunandan, & G. Sivaramakrishna G. (Eds.), *Proceedings of the National Aerospace Propulsion Conference. Lecture Notes in Mechanical Engineering*. Singapore: Springer. doi:10.1007/978-981-15-5039-3\_15
- Dhomne, S., & Mahalle, A. M. (2016). Parameter Optimization of Thermal Barrier Coatings used in Two Stoke Externally Scavenged S.I. Engine using Non-Traditional Optimization Algorithms. *International Journal of Manufacturing, Materials, and Mechanical Engineering*, 6(4), 48–61. doi:10.4018/IJMMME.2016100104
- Djaidir, B., Hafaifa, A., & Kouzou, A. (2017). Faults detection in gas turbine rotor using vibration analysis under varying conditions. *Journal of Theoretical and Applied Mechanics*, 55(2), 393–406. doi:10.15632/jtam-pl.55.2.393
- Donachie, M. J., & Donachie, S. J. (2002). *Superalloys: A technical guide*, #06128G. ASM International. doi:10.31399/asm.tb.stg2.9781627082679
- Efe-Ononeme, O. E., Ikpe, A. E., & Ariavie, G. O. (2018). Modal analysis of conventional gas turbine blade materials (Udimet 500 and IN738) for industrial applications. *Journal of Engineering Technology and Applied Sciences*, 3(2), 119–133.
- Evans, A. G., Mumm, D. R., Hutchinson, J. W., Meier, G. H., & Pettit, F. S. (2001). Mechanisms controlling the durability of thermal barrier coatings. *Progress in Materials Science*, 46(5), 505–553. doi:10.1016/S0079-6425(00)00020-7
- Farrar, C. R., Doebling, S. W., & Nix, D. A. (2021). Vibration-Based Structural Damage Identification. *Philosophical Transactions: Mathematical, Physical and Engineering Sciences*, 359(1778), 131–49.
- Gastaldi, C., Fantetti, A., & Berruti, T. M. (2018). Forced Response Prediction of Turbine Blades with Flexible Dampers: The Impact of Engineering Modelling Choices. *Applied Sciences (Basel, Switzerland)*, 8(1), 34. doi:10.3390/app8010034
- Giridhar, R. K., Ramaiah, P. V., Krishnaiah, G., & Barad, S. G. (2012). Gas Turbine Blade Damper Optimization Methodology. *Advances in Acoustics and Vibration*, 2012, 316761. doi:10.1155/2012/316761
- Hosking, E., Kenny, D. P., McCormick, R. I., Moustapha, S. H., Sampath, P., & Smailys, A. A. (1999). The PW100 engine: 20 years of gas turbine technology evolution. *Proceedings of the RTO Meeting – Design Principles and Methods for Aircraft Gas Turbine Engines*, 8, 4–5.
- Hou, J., Wicks, B. J., & Antoniou, R. A. (2002). An investigation of fatigue failures of turbine blades in a gas turbine engine by mechanical analysis. *Engineering Failure Analysis*, 9(2), 201–211. doi:10.1016/S1350-6307(01)00005-X

- Madhavan, S., Jain, R., Sujatha, C., & Sekhar, A. S. (2014). Vibration based damage detection of rotor blades in a gas turbine engine. *Engineering Failure Analysis*, 46, 26–39. doi:10.1016/j.engfailanal.2014.07.021
- Mevissen, F., & Meo, M. (2019). A review of NDT/structural health monitoring techniques for hot gas components in gas turbines. *Sensors (Basel)*, 19(3), 711. doi:10.3390/s19030711 PMID:30744135
- Nganbe, M. (2009). Strengthening transitions modeling in PM 3030 at intermediate temperature. *Canadian Metallurgical Quarterly*, 48(4), 467–470. doi:10.1179/cm.2009.48.4.467
- Nganbe, M. (2014). Strength and failure of high temperature superalloys. In R. B. Hetnarski (Ed.), *Encyclopedia of Thermal Stresses* (pp. 4579–4591). Springer. doi:10.1007/978-94-007-2739-7\_673
- Nganbe, M., & Fahim, A. (2010). Equicohesion: Intermediate temperature transition of the grain size effect in the nickel-base superalloy PM 3030. *Journal of Materials Engineering and Performance*, 19(3), 395–400. doi:10.1007/s11665-009-9512-9
- Padture, N. P., Gell, M., & Jordan, E. H. (2002). Thermal barrier coatings for gas-turbine engine applications. *Science*, 296(5566), 280–284. doi:10.1126/science.1068609 PMID:11951028
- Palm, W. J. (2007). *Mechanical vibration*. John Wiley.
- Prasad, K., Prasad, B. A., & Anandarao, M. (2017). Material optimization and dynamic approach for performance criteria in application to gas turbine blade to overcome resonance. *International Journal of Scientific and Engineering Research*, 8(6), 189–195.
- Pridorozhnyi, R. P., Zinkovskii, A. P., Merkulov, V. M., Sheremet'ev, A. V., & Shakalo, R. Y. (2019). Calculation-and-Experimental Investigation on Natural Frequencies and Oscillation Modes of Pairwise-Shrouded Cooled Turbine Blades. *Strength of Materials*, 51(6), 817–827. doi:10.1007/s11223-020-00133-6
- Procházka, P., & Vank, F. (2011). Contactless diagnostics of turbine blade vibration and damage. *Journal of Physics: Conference Series*, 305, 012116. doi:10.1088/1742-6596/305/1/012116
- Rani, S., Agrawal, A. K., & Rastogi, V. (2019). Vibration analysis for detecting failure mode and crack location in first stage gas turbine blade. *Journal of Mechanical Science and Technology*, 33(1), 1–10. doi:10.1007/s12206-018-1201-x
- Ranjan, R. (2016). Dynamic Behaviour and Crack Detection of a Multi Cracked Rotating Shaft using Adaptive Neuro-Fuzzy-Inference System: Vibration Analysis of Multi Cracked Rotating Shaft. *International Journal of Manufacturing, Materials, and Mechanical Engineering*, 6(4), 1–10. doi:10.4018/IJMMME.2016100101
- Roemer, M. J., & Kacprzynski, G. J. (2000). Advanced diagnostics and prognostics for gas turbine engine risk assessment. *Proceedings of the 2000 IEEE Aerospace Conference 2000 IEEE Aerospace Conference. Proceedings, Cat. No.00TH8484*, 6, 345–353. doi:10.1109/AERO.2000.877909
- Sankar, V., Ramkumar, P. B., Sebastian, D., Joseph, D., Jose, J., & Kurian, A. (2019). Optimized thermal barrier coating for gas turbine blades. *Materials Today: Proceedings*, 11(3), 912–919. doi:10.1016/j.matpr.2018.12.018
- Saravanamuttoo, H. I. H. (1987). Modern turboprop engines. *Progress in Aerospace Sciences*, 24(3), 225–248. doi:10.1016/0376-0421(87)90008-X
- Schlichting, K. W., Padture, N. P., Jordan, E. H., & Gell, M. (2003). Failure modes in plasma-sprayed thermal barrier coatings. *Materials Science and Engineering A*, 342(1–2), 120–130. doi:10.1016/S0921-5093(02)00251-4
- Sunar, M., & Al-Bedoor, B. O. (2008). Vibration measurement of rotating blades using a root embedded PZT sensor. *Shock and Vibration*, 15(5), 494639. doi:10.1155/2008/494639
- van Dyke, J., & Nganbe, M. (2021). Numerical assessment of blade deflection and elongation for improved monitoring of blade and TBC damage. *Engineering Research Express*, 3(1), 015001. doi:10.1088/2631-8695/abd5a6
- Xu, T., Faulhaber, S., Mercer, C., Maloney, M., & Evans, A. (2004). Observations and analyses of failure mechanisms in thermal barrier systems with two phase bond coats based on NiCoCrAlY. *Acta Materialia*, 52(6), 1439–1450. doi:10.1016/j.actamat.2003.11.025
- Yildirim, M. T., & Kurt, B. (2018). Aircraft gas turbine engine health monitoring system by real flight data. *International Journal of Aerospace Engineering*, 2018, 9570873. doi:10.1155/2018/9570873

*Michel Nganbe received his Ph.D. in 2002 from the Dresden University of Technology in Germany. During his doctoral research, he worked with the Leibniz Institute for Solid State and Materials Research on precipitation- and dispersion-strengthened superalloys. He moved on to work on automotive components development as Test Engineer in Germany from 2001 to 2004. In Canada, he first worked on metal foams development as Research and Development Manager in Montreal, and later on nanostructured coatings as NSERC Industrial Research Fellow in Calgary from 2005 to 2006. He then joined the Department of Mechanical Engineering at the University of Ottawa in Canada as Assistant Professor, and was later promoted to Associate Professor in 2010 and to Full Professor in 2020. Here, his research focuses on theoretical and experimental studies of metallic and ceramic materials, as well as fiber, nanotube and particle reinforced metal- and ceramic-matrix composites for functional, biomedical and structural applications. Targeted industries include aerospace, automotive, transportation, defence, mining, implants, and tools.*